AIP | Journal of Applied Physics

Construction of invisibility cloaks of arbitrary shape and size using planar layers of metamaterials

Oliver Paul, Yaroslav Urzhumov, Christoffer Elsen, David Smith, and Marco Rahm

Citation: J. Appl. Phys. **111**, 123106 (2012); doi: 10.1063/1.4729012
View online: http://dx.doi.org/10.1063/1.4729012
View Table of Contents: http://jap.aip.org/resource/1/JAPIAU/v111/i12
Published by the American Institute of Physics.

Construction of invisibility cloaks of arbitrary shape and size using planar layers of metamaterials

Oliver Paul,[1] Yaroslav Urzhumov,[2] Christoffer Elsen,[1] David Smith,[2] and Marco Rahm[1,3]
[1]*Department of Physics and Research Center OPTIMAS, University of Kaiserslautern, 67663 Kaiserslautern, Germany*
[2]*Center for Metamaterials and Integrated Plasmonics, Pratt School of Engineering, Duke University, Durham, North Carolina 27708, USA*
[3]*Fraunhofer Institute for Physical Measurement Techniques IPM, 79110 Freiburg, Germany*

(Received 28 March 2012; accepted 10 May 2012; published online 20 June 2012)

Transformation optics (TO) is a powerful tool for the design of electromagnetic and optical devices with novel functionality derived from the unusual properties of the transformation media. In general, the fabrication of TO media is challenging, requiring spatially varying material properties with both anisotropic electric and magnetic responses. Though metamaterials have been proposed as a path for achieving such complex media, the required properties arising from the most general transformations remain elusive, and cannot implemented by state-of-the-art fabrication techniques. Here, we propose faceted approximations of TO media of arbitrary shape in which the volume of the TO device is divided into flat metamaterial layers. These layers can be readily implemented by standard fabrication and stacking techniques. We illustrate our approximation approach for the specific example of a two-dimensional, omnidirectional "invisibility cloak," and quantify its performance using the total scattering cross section as a practical figure of merit. © *2012 American Institute of Physics*. [http://dx.doi.org/10.1063/1.4729012]

I. INTRODUCTION

In recent years, the concept of transformation optics (TO) has emerged as a powerful tool for the control and manipulation of light.[1,2] Based on the form-invariance of Maxwell's equations under coordinate transformation, TO is a tool in which the design of electromagnetic materials can be performed conceptually by applying a coordinate transformation to modify the trajectories of waves. By applying the desired coordinate transformation to Maxwell's equations, the prescription for a medium can be obtained for which light propagates as if it was propagating in a different coordinate system.[3] One of the more compelling concepts to emerge from the TO approach has been that of cloaking.[4–11] The TO cloak arises from a transformation in which a region of space is effectively shrunk to a point or singularity, where its scattering becomes significantly reduced. The effect of the transformation is that waves appear to be guided around the "cloaked" region of space, rendering both the bounding TO medium and the cloaked region invisible to an external observer. Since the first experimental realization demonstration of a metamaterial cloak,[5] cloaking devices have been proposed for nearly any imaginable geometry, including spheres,[12,13] circular cylinders,[5,14,15] cylinders of polygonal cross-section,[16–18] and also asymmetric and irregular shapes.[19–23]

Though the coordinate transformations that lead to TO media are often arrived at intuitively and can be simply described, the physical implementation of TO media is typically challenging. In fact, while the mathematics of TO has been known for more than a century, TO has only been deemed relevant in the context of the ongoing development of artificially structured metamaterials over the past decade.[24] TO media are specified by spatially varying distributions of the permittivity and permeability tensors that derive from coordinate transformations. To implement these distributions using metamaterials, the continuously varying constitutive parameters are discretized throughout space and an appropriate metamaterial design is chosen that achieves the desired constitutive tensor elements at each discrete spatial point. Finding the appropriate metamaterial element at each point, however, is a challenging task since nearly arbitrary control is required over each of the electric and magnetic responses along six principal axes. For a given polarization, the number of controlled responses reduces to three for a complete TO solution which still represents a significant challenge. Moreover, in certain circumstances, the required values of the material parameters can get extremely large or even diverge at the boundary of the TO device.[25] Such extreme parameters are almost impossible to implement by common metamaterial structures.

The experimental implementation is further complicated if the cloak possesses curved contours. A conformal cloak designed to conceal a region of arbitrary shape generally leads to a curvilinear alignment of the principal axes of the permittivity and permeability tensors, resulting in a gradual rotation of the local metamaterial cells throughout space. The metamaterial architecture for such designs can be surprisingly complex in all but the most symmetric designs. Even for highly symmetric designs, such as that of a spherical metamaterial, the fabrication can pose a significant hurdle. Since most fabrication techniques are suited for the production of planar samples, it is of considerable advantage to seek approximation methods that will leverage standard and commercial lithographic patterning.[24] For TO devices operating at microwave[5] and THz (Ref. 26) frequencies, cylindrical device shapes can be obtained by curling planar

sheets of metamaterials. However, as the operational frequency increases towards the optical range and the metamaterial layer thickness decreases to micro- and nanometer scale, this approach becomes impractical. For TO devices with fully three-dimensional shapes, such as spherical cloaks, curving planar-layer metamaterials is not a viable approach even for microwave frequencies. While substantial progress is being made towards volumetric three-dimensional metamaterial fabrication methods,[24] the contemporary techniques remain prohibitively difficult to use for structures that cannot be conceived as "sandwiched" flat layers of meta-elements. For three-dimensional TO devices such as the one shown in Fig. 1 faceted approximations are therefore essential.

In this paper, we present an approximation method that overcomes these fabrication hurdles and enables the construction of TO media with planar layers of metamaterials. We start by the observation that every arbitrary TO medium which may have curved surfaces can be substituted by a polygonal (in two dimensions) or polyhedral (in 3D) approximation. Clearly, as the number of vertices increases, the error in the approximation should decrease, and eventually becoming negligible. Next, a coordinate transformation is applied to the polygonal approximation to calculate the spatial distribution of the permittivity and permeability tensors. The resulting tensor distribution mirrors the architecture of the required metamaterial realization. In three consecutive approximations, we then reduce the complexity of the individual metamaterial cells, align the cells in plan-parallel layers and simplify the spatial distribution of the material parameters. The performed reduction of the metamaterial architecture also eliminates the need of extremely large values of the permittivity or permeability and allows the usage of common metamaterial structures. As a result, the original TO medium (with possibly curved surfaces) is replaced by an approximative TO structure that is composed by plan-parallel, flat layers of simplified metamaterial elements. Such layers can be readily constructed by standard lithographic and stacking techniques.

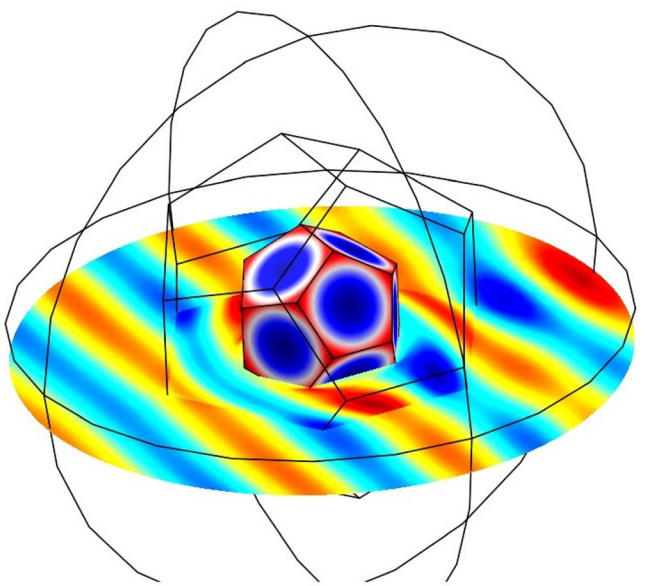

FIG. 1. Full-wave simulation: faceted dodecahedral approximation to the full-parameter spherical cloak, obtained by truncating the sphere circumscribing a regular dodecahedron. No correction to the material property distribution was made.

In the following, we explain and demonstrate the proposed approximation method for the example of a polygonal invisibility cloak. The metamaterial invisibility cloak provides a useful structure for investigating the performance of layered approximations because it can be well-characterized by a single figure-of-merit: the (total) scattering cross-section (SCS).[27,28] For this reason, we choose the cloaking transformation as illustrative example testing the performance of the layered approximations.

II. TRANSFORMATION OPTICS OF POLYGONAL CLOAKS

We restrict our analysis to two-dimensional (in-plane) wave propagation through a cylindrical invisibility cloak whose cross-section is formed by a regular N-sided polygon and whose cylinder axis coincides with the z-axis. For the incident wave, we consider a monochromatic TE-wave propagating in the x-direction according to

$$\boldsymbol{E}(x,t) = E_0 e^{i(kx-\omega t)}\hat{\boldsymbol{z}}, \tag{1}$$

with the electric field amplitude E_0, the wave vector k and the angular frequency ω.

For the implementation of a polygonal cloak, we apply a very general transformation technique which is applicable to a large class of geometries.[20] The technique does not require a certain symmetry like in a circular-cylindric cloak,[5,6] and, in fact, is also applicable to geometries that do not possess any symmetry at all. The only requirement is that the inner and outer boundaries of the cloak can be parameterized in polar coordinates as

$$r = R_{1,2}(\phi), \tag{2}$$

where the indexes 1 and 2 refer to the inner and the outer surfaces, respectively. For example, regular polygons with N sides can be parameterized as follows:

$$r = \frac{r_i}{\cos(\phi \bmod (2\pi/N) - \pi/N)}, \tag{3}$$

where r_i is the inradius of the polygon, i.e., the radius of the inscribed circle of the polygon. The cloak domain (where the constitutive parameters differ from vacuum) occupies the area described in cylindrical coordinates by $R_1(\phi) < r < R_2(\phi)$. The coordinate transformation that compresses the cross-section of the inner surface to zero can be chosen as follows:

$$r' = \frac{R_2(\phi)}{R_2(\phi) - R_1(\phi)}(r - R_1(\phi)), \quad \phi' = \phi. \tag{4}$$

Since the transformation (4) depends on both r and ϕ, the ϵ and μ tensors of the cloak are no longer aligned with the $\hat{r}$ and $\hat{\phi}$ directions of the cylindrical coordinates. Therefore, the expressions for the tensor components are equally involved in cylindrical and Cartesian coordinates. Since our

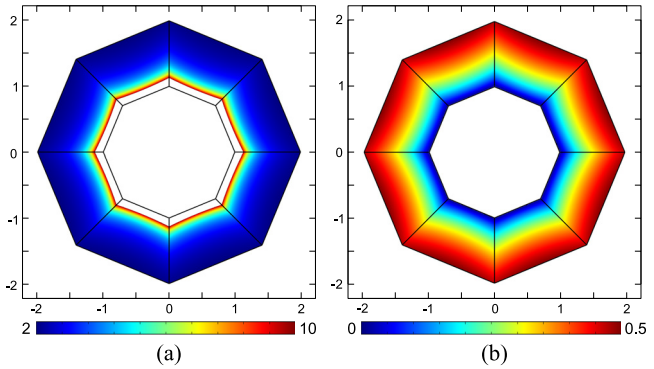

FIG. 2. (a) Distribution of the first and (b) second principal values of the in-plane μ tensor in the cloak derived from the exact coordinate transformation of an octagon-shaped cloak according to Eq. (6). Note that the first principal values diverge at the inner boundary of the cloak.

electromagnetic solver requires material tensor input in Cartesian coordinates, the transformation (4) must be expressed in Cartesian coordinates of the form $x = x(x', y')$ and $y = y(x', y')$. This is achieved by applying the intermediate transformations $x = r\cos\phi$ and $y = r\sin\phi$ in the unprimed system and the inverse intermediate transformations $r' = \sqrt{x'^2 + y'^2}$ and $\phi' = \arctan(y'/x')$ in the primed system, respectively. In the Cartesian system, we can then calculate the Jacobian matrix of the transformation defined as $A^i_{j'} = \partial x^i / \partial x^{j'}$ with $i, j = 1, 2$ (assuming $x_1 \equiv x$ and $x_2 \equiv y$). Once the Jacobian matrix is found, the constitutive material parameters for the cloak medium are obtained by

$$\epsilon^{ij} = \mu^{ij} = \det(A)^{-1} A^i_{i'} A^j_{j'} \delta^{i'j'}, \tag{5}$$

where we used the Einstein sum convention of summing over identical indices. After a straightforward algebraic calculation, this yields the following expressions of a two dimensional, polygonal cloak (TE-polarization):

$$\begin{aligned}
\mu_{xx} &= \frac{1}{\alpha r r'}(r\sin\phi - \beta\cos\phi)^2 + \frac{\alpha r'}{r}\cos^2\phi, \\
\mu_{yy} &= \frac{1}{\alpha r r'}(r\cos\phi + \beta\sin\phi)^2 + \frac{\alpha r'}{r}\sin^2\phi, \\
\mu_{xy} &= \left(\frac{\alpha r'}{r} - \frac{r}{\alpha r'} + \frac{\beta^2}{\alpha r' r}\right)\sin\phi\cos\phi + \frac{\beta}{\alpha r'}\cos(2\phi) = \mu_{yx}, \\
\epsilon_{zz} &= \frac{r'}{\alpha r}.
\end{aligned} \tag{6}$$

The remaining expressions for r', α, and β depend on the particular geometry of the polygonal cloak. If the inner and outer boundaries of the cloak are regular, N-sided polygons with inradius a and b, respectively, these expressions are given by

$$r' = \frac{b}{b-a}\left(r - \frac{a}{\cos(\Phi)}\right), \quad \alpha = \frac{b-a}{b}, \quad \beta = a\frac{\sin(\Phi)}{\cos^2(\Phi)}, \tag{7}$$

where $\Phi = \phi \bmod (2\pi/N) - \pi/N$ is the angle between the position vector $\mathbf{r}$ and the middle axis of the polygon section in which the considered point is located. Note that in the limit $N \to \infty$, the angle Φ and thus β tends to zero and the resulting material parameters approach those of a circular-cylindric cloak as expected.[25] The resulting distribution of the in-plane μ tensor of an octagonal cloak is exemplarily plotted in Fig. 2.

III. APPROXIMATIONS TOWARDS A METAMATERIAL IMPLEMENTATION

TO devices can often be realized by collections of metamaterial cells, each designed to provide a local response that approximates the permittivity and permeability tensors at that point. The first step, then, towards implementation of the TO device is the spatial discretization of the otherwise continuous permittivity and permeability distributions. After having accomplished a reasonable discretization, the values of the permittivity and permeability tensors can then be realized by design of the metamaterial cells. However, as discussed in the Introduction, the spatial arrangement of the cells within the metamaterial represents an impediment to the manufacturability of the TO device. Furthermore, even for the simplest case of a two dimensional, cylindrical cloak, the exact transformation requires a careful control over four independent tensor components throughout space (with eventually diverging values) which also hampers an experimental realization.

In order to overcome these technological hurdles, we present in the following three different approximations of a polygonal cloak which provide a stepwise reduction of the complexity of the required metamaterial architecture and, thus, enable a practical realization of a cloaking device with state-of-the-art fabrication abilities. The three approximations, denoted as APX 1, APX 2, and APX 3, are depicted in Fig. 3 and are implemented in the numeric model as explained below.

A. APX 1: Eikonal approximation

The complete parameter set for a polygonal cloak given by Eq. (6) dictates the control of four independent tensor components throughout space which is very difficult to realize in practice. Therefore, in our first approximation APX 1, we replace the exact material parameters by a reduced parameter set in which one of the principal values of the in-plane μ tensor is set constant. This approximation is known as the *eikonal approximation* and is based on the fact that for the wave propagation inside the cloak only the refractive indices given by $n_\phi = \sqrt{\epsilon_z \mu_r}$ and $n_r = \sqrt{\epsilon_z \mu_\phi}$ are relevant.[5,29–31] Here μ_r and μ_ϕ denote the eigenvalues of the μ tensor[32] associated with the local eigenvector basis $\{\mathbf{e}_r, \mathbf{e}_\phi\}$ as depicted in Fig. 3(b). An eikonal cloak can be derived from an exact cloak in an infinite number of ways. Here, we fix $\mu^{\text{eik}}_\phi \equiv 1$, in which case the cloak is described by

$$\epsilon^{\text{eik}}_z = \epsilon_z \mu_\phi, \quad \mu^{\text{eik}}_r = \mu_r / \mu_\phi, \quad \mu^{\text{eik}}_\phi = 1. \tag{8}$$

With the reduced parameter set, the ray trajectories inside the cloak are the same as in the exact cloak, however, the surface of the cloak may have a nonzero reflectance due to

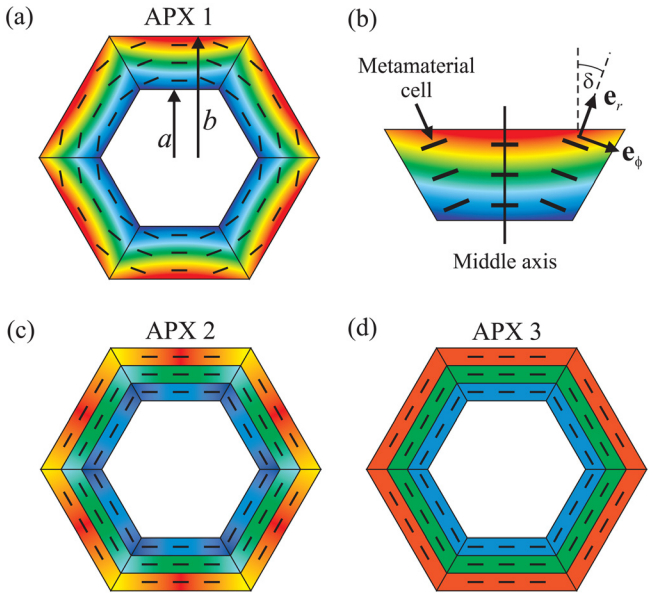

FIG. 3. Overview over the three approximations APX 1 to APX 3. The color gradient visualizes the spatial distribution of the principal values of the material tensors (here μ_r^{eik} for instance) whereas the short lines indicate the spatial orientation of the metamaterial cells. (a) APX 1: Reduction of the cell architecture by using an eikonal approximation. (b) Enlarged polygon sector of APX 1. (c) APX 2: Alignment of the metamaterial cells along flat layers. (d) APX 3: Usage of identical metamaterial cells within each layer.

the impedance mismatch.[5,33] To mitigate the wave reflectance on the surface,[5,33] additional steps can be taken.[29,33] Since one principal value of the permeability is set to unity, the eikonal approximation corresponds to a simplified metamaterial structure in which the unit cell possesses a magnetic response in only one direction. Such metamaterial cells can be realized by flat metallic patterns like the split ring resonators used in Ref. 5 and are much easier to fabricate than those with two independent magnetic dipoles in different directions.

Note that the eikonal approximation (8) refers to the local eigenvalues of the μ tensor whereas the tensor elements derived in Eq. (6) refer to the Cartesian coordinate system which, in general, does not serve as an eigenbasis for μ. Consequently, in order to apply the eikonal approximation to our polygonal cloak, we have to determine the local eigenbasis of the μ tensor at each point of the cloak volume and then perform the eikonal approximation according to Eq. (8). For example, for points located at the middle axis of a polygon section, this yields the following expressions:

$$\epsilon_z^{\text{eik}} = \left(\frac{b}{b-a}\right)^2, \quad \mu_r^{\text{eik}} = \left(\frac{r-a}{r}\right)^2, \quad \mu_\phi^{\text{eik}} = 1. \tag{9}$$

Subsequently, in order to implement the eikonal approximation in our solver environment, we have to re-express the μ^{eik} tensor in the Cartesian coordinate system.

A further advantage of the eikonal approximation is that it eliminates any infinite values of the tensor components which usually occur at the inner boundary of a cloak.[25] For instance, all tensor components described by Eq. (9) remain finite.

B. APX 2: Alignment of the metamaterial cells

In the second approximation APX 2, we assume that the eikonal approximation of the cloak has already been established and refer to the reduced parameter set of Eq. (8). In addition to that, we assume that all metamaterial cells are rotated about the z-axis such that the eigenvectors of the μ-tensor are aligned to be parallel and orthogonal to the outer boundary of the polygon as schematically visualized in Fig. 3(c). The resulting uniform alignment of the cells within one polygon section allows a subdivision of the sections into flat, plan-parallel layers which are significantly easier to fabricate than bulk metamaterials with locally varying orientation of its elements. By stacking these pre-fabricated layers, the polygonal cloak can be readily constructed.

In the numerical model, the rotation of the metamaterial cells is implemented by applying a rotation matrix $R(\delta)$ to the μ^{eik} tensor at each point of the cloak volume (ϵ_z^{eik} remains unchanged) according to

$$\mu^{\text{eik,rot}} = R(\delta)^T \mu^{\text{eik}} R(\delta), \tag{10}$$

with the rotation matrix

$$R(\delta) = \begin{pmatrix} \cos\delta & -\sin\delta \\ \sin\delta & \cos\delta \end{pmatrix}. \tag{11}$$

In this notation, the tensor μ^{eik} is expressed in Cartesian coordinates and δ is the angle between the radial principal axis of the considered metamaterial cell (i.e., the $\mathbf{e}_r$ eigenvector of μ^{eik}) and the middle axis of the polygon section in which the element is located (see Fig. 3(b)). As a result, the rotation misalignment of the metamaterial cells with respect to the middle axis is removed and thus all metamaterial cells in a given polygon section have the same orientation (see Fig. 3(c)).

Furthermore, in order to account for the discretization of the cloak volume into flat layers, the material parameters were calculated only at the middle plane of each layer and then kept constant across the layer thickness. In other words, the material parameters in APX 2 vary only in the direction parallel to the layers as depicted by the color gradient in Fig. 3(c). This introduces a discontinuity of the material properties at the interface between adjacent layers which is naturally present in any layered composite.

C. APX 3: Homogenization of the layers

By now, the metamaterial cells possess a reduced complexity and are uniformly aligned along flat layers. However, the geometric dimensions of the metamaterial cells still vary within these layers. In our final approximation APX 3, we drop this requirement and assume that all layers are completely homogeneous as schematically visualized in Fig. 3(d). This approximation further facilitates the fabrication process since no effort for the relative alignment of subsequent layers is necessary. To implement APX 3 in the numeric model, we calculated the material parameters μ^{eik} and ϵ^{eik} at the center point of each layer and then kept the resulting values constant within the entire layer. As in

APX 2, all metamaterial cells are equally aligned in each polygon section.

IV. SIMULATION RESULTS AND DISCUSSION

In order to quantify the validity of the different approximations APX 1 to APX 3, we performed numerical calculations and determined the SCS for an exact polygonal cloak as well as the approximate realizations APX 1 to APX 3. In the simulation, the cloak core was filled with a quasi-perfect electrical conductor with a conductivity of 10^{16} S/m. To verify the appropriateness of the numerical model, we present in Figs. 4(a) to 4(d) the simulated field distribution for an incident plane wave for the uncloaked core, the exact polygonal cloak and, exemplarily, for the two approximations APX 2 and APX 3, respectively. The plots confirm that both approximations reduce the backscattering as well as the forward scattering leading to a field pattern that is qualitatively comparable to that of the exact cloak.

For a quantitative description of the proposed approximations, we calculated the SCS of the differently approximated cloaks for an incident plane wave.[28] According to the optical theorem in two dimensions,[34] the total cross-section (which includes absorption and scattering) can be determined from the forward scattering amplitude $f(0)$

$$\sigma_{tot} \equiv \sigma_{sc} + \sigma_{abs} = -2\sqrt{\lambda}\mathrm{Re}\{\sqrt{i}f(0)\}, \qquad (12)$$

where λ is the wavelength in the medium surrounding the scatterer—in our case, the free space wavelength. The scattering amplitude depends only on the scattering angle and is defined by the asymptotic formula

$$E(r,\phi) \sim E_0\left(e^{ikr} + \frac{f(\phi)}{\sqrt{r}}e^{ikr}\right), \quad r \to \infty, \qquad (13)$$

in which r is the distance from the scatterer, E_0 is the amplitude of the incident plane wave, and $k = 2\pi/\lambda$ is the wave number. Thus, in two dimensions $f(\phi)$ has the units of $(\text{length})^{1/2}$, and σ_{tot} has the units of length. For a lossless scatterer, $\sigma_{abs} = 0$ and thus the optical theorem yields the SCS (σ_{sc}) directly without additional calculations. Our simulation software allows the calculation of the far-field amplitude in the forward scattering direction; that quantity is linearly proportional to the forward-scattering amplitude in Eq. (12), which permits us to perform an inexpensive calculation of the total SCS. In the following, we present the SCS for the three approximations APX 1 to APX 3 as a function of the size of the cloaked area, the cloak shell thickness, the number of polygon sides and layers, and the angle of wave incidence. All calculations refer to the incident TE-wave specified in Eq. (1) with fixed frequency ω.

A. Influence of the size of cloak

To evaluate the limitations of the proposed models, we first calculated the SCS as a function of the size of the cloak. For this purpose, we varied the radius of the cloaked area from $a = 0.5\lambda$ to $a = 3.5\lambda$ while the outer radius of the cloak was proportionally increased according to $b = 2a$. The assumed cloak geometry was a 10-sided polygon and for the layered models APX 2 and APX 3, the number of layers was

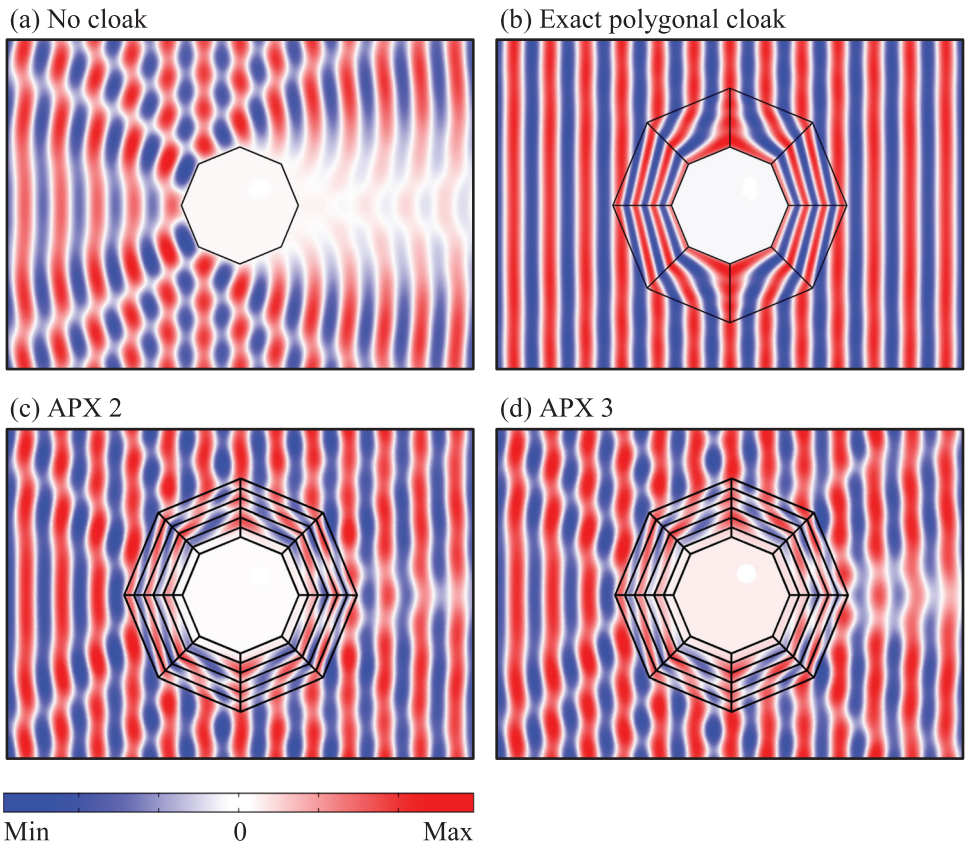

FIG. 4. Simulation results for the z-component of the electric field of a TE-wave incident from the left for (a) the bare conducting object without cloak, (b) the polygonal cloak with the exact transformations, (c) approximation APX 2, and (d) APX 3.

stepwise increased (starting from 5 layers) in order to keep the layer thickness smaller than $\lambda/10$. The corresponding material parameters are obtained from the transformations discussed in Secs. II, and III. For the specified dimensions, the material parameters cover the range

$$\epsilon_z^{\text{eik}} \approx 4,\ 0 \le \mu_r^{\text{eik}} \le 0.25, \quad \mu_\phi^{\text{eik}} = 1. \tag{14}$$

Obviously, the used eikonal approximation eliminates the need of extraordinary large material parameters which usually occur for metamaterial realizations of invisibility cloaks.[2,25] For our implementations, the required material parameters are restricted to realistic values which can be readily obtained by common metamaterial structures.[5] It should be noted that the covered parameter range only depends on the ratio b/a and thus is identical for all investigated cloak sizes (for points located at the middle axis of a polygon section this can be verified by Eq. (9)). In other words, all analyzed cloak sizes can be realized by the same set of metamaterial cells which provides a reasonable comparison of the different models.

In Fig. 5, we show the resulting SCS normalized to the SCS of the bare conducting core for all three approximations. In order to validate the accuracy of the SCS calculation, we have also plotted the SCS of a polygonal cloak that is implemented by the exact material parameters (black line in Fig. 5). As expected, the resulting values of the SCS for the exact cloak are almost zero. The red, blue, and green curves in Fig. 5 show that all three models provide a reasonable cloaking performance with a significant reduction of the SCS. Obviously, the scattering of the models APX 1 and APX 2 is almost independent of the size of the cloak with values of the normalized SCS between 0.20 and 0.35. In contrast, model APX 3 is more sensitive to the cloak size and shows a slight increase of the SCS from 0.30 to 0.54 as the inner radius of the cloaked area increases from $a = 0.5\lambda$ to $a = 3.5\lambda$. The increasing SCS for model APX 3 is a direct consequence of the stronger approximations made in this model. As shown later, this can be compensated by increasing the number of polygon edges.

Once the area to be cloaked is specified, the cloak can still be optimized by varying the size of the cloak shell. Therefore, we determined the cloaking performance of the different approximations with respect to the thickness of the cloak shell $(b-a)$ for a constant inner radius of $a = 2\lambda$ and for a 10-sided polygon. Again, the number of layers in APX 2 and APX 3 was stepwise increased to keep the layer thickness smaller than $\lambda/10$. The resulting SCS of the three approximations in dependence on the normalized shell thickness $(b-a)/\lambda$ is plotted in Fig. 6.

The total dependence of the SCS on the cloak shell thickness is a combination of two contrary effects. First, as discussed in Sec. III, all approximations are based on a reduced parameter set which implies a non-zero reflectance of the cloak's surface. The corresponding wave impedance at the surface of the cloak is approximately

$$z^{\text{eik}} = \sqrt{\mu_\varphi^{\text{eik}}/\epsilon_z^{\text{eik}}} \approx 1 - a/b. \tag{15}$$

Consequently, the wave impedance approaches that of free space as the radius of the outer boundary b increases (a is fixed) which leads to a decreasing scattering. This behavior is shown by the SCS of model APX 1 (blue line in Fig. 6) which strictly decreases from 0.77 to 0.14 as the cloak shell thickness increases from 0.2λ to 4λ. On the other hand, an increasing cloak shell thickness implies that the role of spatial imperfections introduced by the approximations gain significance, especially at the corners of the polygon. This leads to an increasing scattering which partly compensates the improved impedance matching. As a result, the SCS of model APX 2 and APX 3 which include stronger approximations than APX 1 decreases only moderately as the cloak shell increases (see red and green curves in Fig. 6). At a shell thickness of about 4λ, the two counter effects of the increasing imperfections and the improving impedance matching are almost balanced and the SCS of

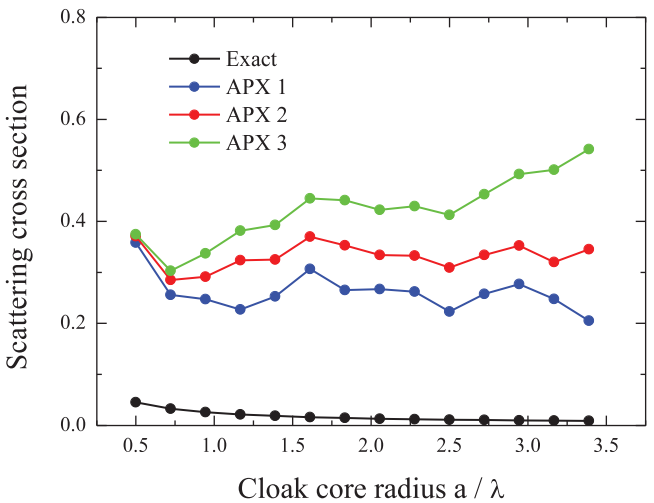

FIG. 5. SCS normalized to the SCS of the bare conducting core for the proposed approximations APX 1 to APX 3 in dependence on the cloak core radius a. The simulations refer to a 10-sided polygonal cloak with an outer cloak radius of $b = 2a$. The black line indicates the SCS of an exact polygonal cloak.

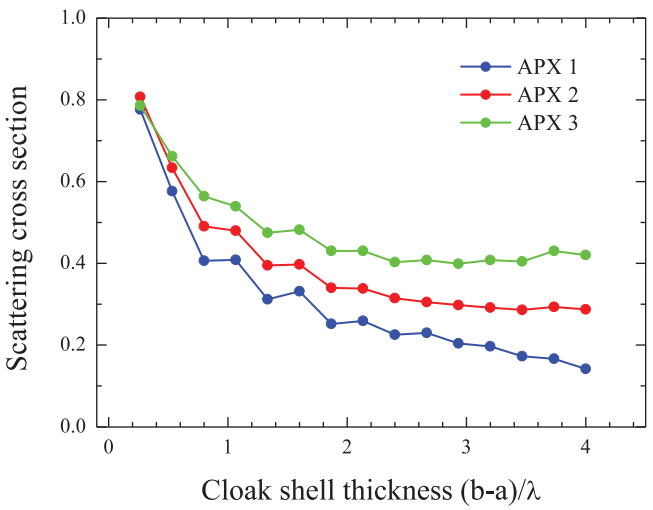

FIG. 6. Normalized SCS of APX 1 to APX 3 in dependence on the cloak shell thickness. The considered cloak geometry is a 10-sided polygon with an inner radius of $a = 2\lambda$.

APX 2 and APX 3 approaches a value of SCS = 0.28 and SCS = 0.41, respectively

B. Influence of the number of polygon sides and number of layers

In order to estimate the fabrication effort of a polygonal cloak, we next investigated the impact of the number of polygon sides N on the cloaking performance. For this purpose, we calculated the SCS as a function of N for the example of a cloak with an inner and outer radius of $a = 2\lambda$ and $b = 4\lambda$, respectively. The resulting SCS of the models APX 1 to APX 3 is plotted in Fig. 7. Obviously, model APX 1 is nearly independent of N with a constant SCS around 0.25. This stable behavior is related to the fact that the eikonal approximation used for APX 1 only affects the reflectance of the cloak's boundary while the wave trajectory inside the cloak is identical to that of the exact polygonal cloak. Since the performance of the latter is independent of the number of polygon sides, the same also holds for APX 1. In contrast, approximations APX 2 and APX 3 introduce spatial imperfections inside the cloak volume which increase with the size of the angle $2\pi/N$ a polygon section spans (see Fig. 3). Consequently, if N increases the spatial imperfections decreases and the SCS of both APX 2 and APX 3 decreases as well and approaches the scattering of APX 1. At a threshold of about 12 polygon sides, we observed no significant difference between the three models.

A further fabrication issue for a successful realization of a layered cloak is the number of layers that is necessary to provide a reasonable cloaking effect. In Fig. 8, we show the normalized SCS as a function of layer package density, exemplarily plotted for model APX 2. The assumed geometry of the cloak was an 8-sided polygon with an inner radius of $a = 2\lambda$ and an outer radius of $b = 4\lambda$. As expected, the curve shows a fast convergence towards a constant SCS which corresponds to a quasi-continuous distribution of the material parameters. A sufficient convergence is already achieved for a package density of about 8 layers per wavelength. For more than 11 layers, the difference to the quasi-continuous limit is

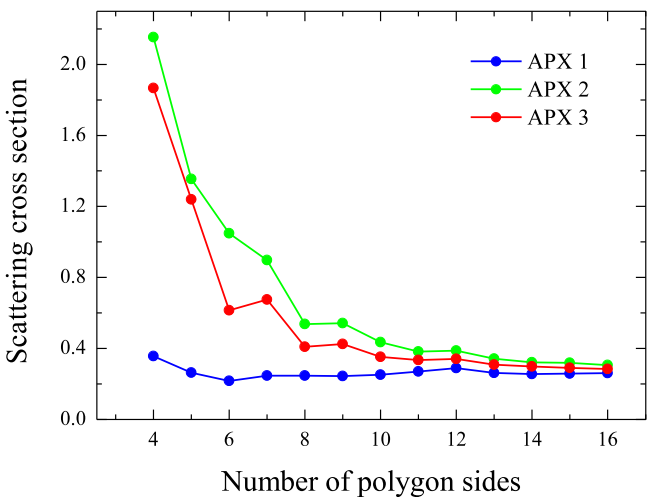

FIG. 7. Normalized SCS for a polygonal cloak with an inner radius of $a = 2\lambda$ and outer radius $b = 4\lambda$ in dependence on the number of polygon sides.

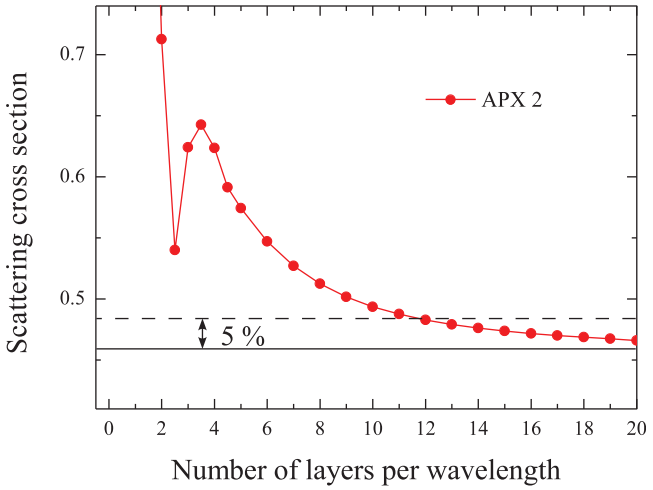

FIG. 8. Normalized SCS for a polygonal cloak with an inner radius of $a = 2\lambda$ and an outer radius $b = 4\lambda$ in dependence on the layer package density for model APX 2. The dashed line indicates the region where the SCS differs from the SCS of the quasi-continuous limit by less than 5%.

less than 5% (see Fig. 8). This condition is usually satisfied in common metamaterial implementations.

The local minimum at 2.5 layers per wavelength corresponds to a reduced reflection of the cloak caused by destructive interference of waves that are partly reflected at different layers. This interference minimum, however, is not stable and critically depends on the considered frequency and the angle of wave incidence.

C. Influence of the angle of incidence

As a final aspect of the proposed polygonal approximations, we analyzed the influence of the orientation of the cloak with respect to the incident wave. This dependence is exemplarily shown in Fig. 9 where we have plotted the normalized SCS of the models APX 1 to APX 3 as a function of the angle of wave incidence (an angle of 0° corresponds to the case where the wave impinges normally to a polygon side). The calculations refer to a polygonal cloak with an

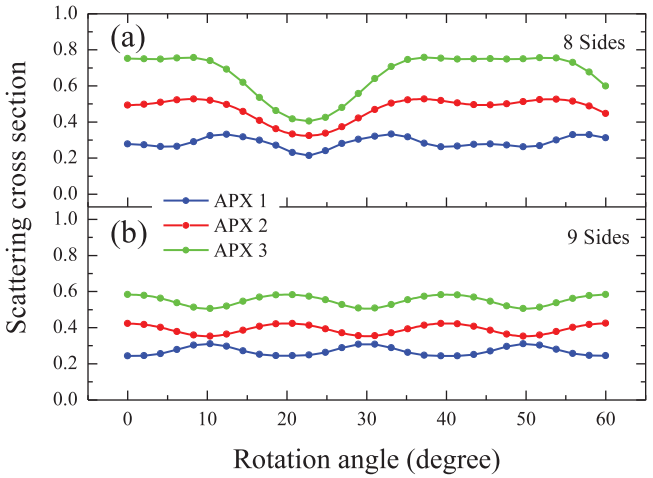

FIG. 9. Normalized SCS in dependence on the angle of wave incidence for (a) an 8-sided polygonal cloak and (b) a 9-sided polygonal cloak. The angle of 0° corresponds to the case where the impinges normally to a polygon side.

inner and outer radius of $a = 2\lambda$ and $b = 4\lambda$, respectively, and we considered an 8-sided polygon (Fig. 9(a)), as well a 9-sided polygon (Fig. 9(b)).

The resulting curves show a periodic modulation which mirrors the annular period of a regular polygon. Obviously, the angle sensitivity of a 9-sided polygon is smaller than that of an 8-sided polygon. For example, the SCS of model APX 2 varies from 0.32 to 0.52 if the cloak is an 8-sided polygon but only from 0.35 to 0.42 if the cloak consists of 9 polygon sides (red lines in Figs. 9(a) and 9(b)). The reason for the reduced angle sensitivity is the odd number of polygon sides as can be explained as follows: there are two symmetric orientations of a polygonal cloak with respect to the incident wave. The first occurs if a polygon side is normal to the incident wave (case 1) and the second occurs if a vertex of the polygon points towards the source (case 2). If the polygon has an even number of sides the two cases possess strongly different SCS because the front and the back of the cloak are defined by either two parallel sides (case 1) or two opposing vertices (case 2). However, if the number of polygon sides is odd, a side is always opposite to a vertex and thus the two cases have a comparable geometry. This leads to similar values of the SCS and thus to a reduced angle dependence.

In the case of the 9-sided, polygonal cloak to which Fig. 9(b) refers, the standard deviation from the annularly averaged SCS is less then 10% for all three models APX 1 to APX 3. Hence, if the number of polygon edges is not too small, the omnidirectional cloaking ability of the exact polygonal cloak is still well maintained by the proposed approximations.

V. CONCLUSION

In this paper, we proposed an approximation method for a practical realization of TO components of arbitrary shape by flat layers of metamaterials. The proposed method starts from a polygonal approximation of a possibly curved shape for which an exact coordinate transformation can be established. In three consecutive approximations, we reduced the complexity of the metamaterial cells required for the exact transformation (APX 1), arranged the cells in plan-parallel layers (APX 2), and simplified the spatial material distribution within these layers (APX 3). As a major advantage, the polygonal approximation significantly mitigates the fabrication constraints since the resulting TO components can be implemented by flat metamaterial layers. This can be readily achieved by standard lithographic and stacking techniques.

We have validated the proposed method for the example of a polygonal invisibility cloak and quantified the accuracy of the approximations by comparing the SCS of the cloak with that of an exact polygonal cloak. All three introduced approximations showed a comparable and reasonable cloaking performance. For instance, for a cloaked area with a diameter of 4λ and realistic geometric dimensions, we achieved a reduction of the SCS down to 14% of the uncloaked core.

In a detailed parametric study, we have investigated the performance of the models in dependence on different geometric variables such as the number of polygon edges, the cloak shell thickness and the number of metamaterial layers. In this context, we have also shown that the omnidirectional cloaking ability of the exact circular-cylindrical cloak is well maintained by the introduced flat-face approximations. Such flat layers can be manufactured even with micro- and nanoscale dimensions by standard fabrication techniques.

The presented method enables the construction of TO media in the high frequency range and is also applicable for the realization of three-dimensional TO devices.

ACKNOWLEDGMENTS

This work was partially supported through a Multidisciplinary University Research Initiative, sponsored by the U.S. Army Research Office (Contract No. W911NF-09-1-0539).

[1]J. B. Pendry, D. Schurig, and D. R. Smith, Science **312**, 1780 (2006).
[2]M. Rahm, S. A. Cummer, D. Schurig, J. B. Pendry, and D. R. Smith, Phys. Rev. Lett. **100**, 063903 (2008).
[3]N. Kundtz, D. Smith, and J. Pendry, Proc. IEEE **99**, 1622 (2011).
[4]A. Greenleaf, M. Lassas, and G. Uhlmann, Physiol. Meas. **24**, 413 (2003).
[5]D. Schurig, J. J. Mock, B. J. Justice, S. A. Cummer, J. B. Pendry, A. F. Starr, and D. R. Smith, Science **312**, 977 (2006).
[6]W. Cai, U. K. Chettiar, A. V. Kildishev, and V. M. Shalaev, Nat. Photonics **1**, 224 (2007).
[7]R. V. Kohn, H. Shen, M. S. Vogelius, and M. I. Weinstein, Inverse Probl. **24**, 015016 (2008).
[8]A. Greenleaf, Y. Kurylev, M. Lassas, and G. Uhlmann, New J. Phys. **10**, 115024 (2008).
[9]C. Qiu, L. Hu, B. Zhang, B.-I. Wu, S. G. Johnson, and J. D. Joannopoulos, Opt. Express **17**, 13467 (2009).
[10]N. I. Landy, N. Kundtz, and D. R. Smith, Phys. Rev. Lett. **105**, 193902 (2010).
[11]U. Leonhardt, Nature **471**, 292293 (2011).
[12]A. Novitsky, C.-W. Qiu, and S. Zouhdi, New J. Phys. **11**, 113001 (2009).
[13]C.-W. Qiu, L. Hu, X. Xu, and Y. Feng, Phys. Rev. E **79**, 047602 (2009).
[14]Z. Ruan, M. Yan, C. W. Neff, and M. Qiu, Phys. Rev. Lett. **99**, 113903 (2007).
[15]D.-H. Kwon and D. H. Werner, Appl. Phys. Lett. **92**, 013505 (2008).
[16]Q. Wu, K. Zhang, F.-Y. Meng, and L.-W. Li, J. Phys. D: Appl. Phys. **42**, 035408 (2009).
[17]M. Rahm, D. Schurig, D. A. Roberts, S. A. Cummer, D. R. Smith, and J. B. Pendry, Photonics Nanostruct. Fundam. Appl. **6**, 87 (2008).
[18]B.-I. Popa and S. A. Cummer, Phys. Rev. A **82**, 033837 (2010).
[19]T. Han, C. Qiu, and X. Tang, J. Opt. **12**, 095103 (2010).
[20]A. Nicolet, F. Zolla, and S. Guenneau, Opt. Lett. **33**, 1584 (2008).
[21]C. Li and F. Li, Opt. Express **16**, 13414 (2008).
[22]W. X. Jiang, J. Y. Chin, Z. Li, Q. Cheng, R. Liu, and T. J. Cui, Phys. Rev. E **77**, 066607 (2008).
[23]X. Wang, S. Qu, S. Xia, B. Wang, Z. Xu, H. Ma, J. Wang, C. Gu, X. Wu, L. Lu, and H. Zhou, Photonics Nanostruct. Fundam. Appl. **8**, 205 (2010).
[24]C. M. Soukoulis and M. Wegener, Nat. Photonics **5**, 523 (2011).
[25]S. A. Cummer, B.-I. Popa, D. Schurig, D. R. Smith, and J. B. Pendry, Phys. Rev. E **74**, 036621 (2006).
[26]H. Tao, A. C. Strikwerda, K. Fan, C. M. Bingham, W. J. Padilla, X. Zhang, and R. D. Averitt, J. Phys. D: Appl. Phys. **41**, 232004 (2008).
[27]N. B. Kundtz, D. Gaultney, and D. R. Smith, New J. Phys. **12**, 043039 (2010).
[28]Y. A. Urzhumov, N. B. Kundtz, D. R. Smith, and J. B. Pendry, J. Opt. **13**, 024002 (2011).
[29]Y. Urzhumov, F. Ghezzo, J. Hunt, and D. R. Smith, New J. Phys. **12**, 073014 (2010).
[30]Y. A. Urzhumov and D. R. Smith, Phys. Rev. Lett. **105**, 163901 (2010).
[31]Y. Urzhumov and D. R. Smith, in *Proceedings of the 5th International Congress on Advanced Electromagnetic Materials in Microwaves and Optics*, 2011.
[32]We chose the label r and ϕ for the eigenvectors and the eigenvalues of the μ tensor since the eigenvectors $\mathbf{e}_r$ and $\mathbf{e}_\phi$ point approximately in the radial and azimuthal direction, respectively.
[33]W. Cai, U. K. Chettiar, A. V. Kildishev, V. M. Shalaev, and G. W. Milton, Appl. Phys. Lett. **91**, 111105 (2007).
[34]L. J. Boya and R. Murray, Phys. Rev. A **50**, 4397 (1994).